NIH Public Access
Author Manuscript
Genesis. Author manuscript; available in PMC 2014 September 01.

Published in final edited form as:
Genesis. 2013 September ; 51(9): 667–675. doi:10.1002/dvg.22407.

Troponin T3 expression in skeletal and smooth muscle is required for growth and postnatal survival: Characterization of *Tnnt3*$^{tm2a(KOMP)Wtsi}$ mice

Yawen Ju, M.S.[1,2], **Jie Li, Ph.D**[1], **Chao Xie, M.D.**[1,2], **Christopher T. Ritchlin**[1,3], **Lianping Xing, Ph.D.**[1,2], **Matthew J. Hilton, Ph.D.**[1], and **Edward M. Schwarz, Ph.D.**[1,2,4]

[1]Center for Musculoskeletal Research, University of Rochester School of Medicine and Dentistry, Rochester, NY

[2]Department of Pathology and Laboratory Medicine, University of Rochester School of Medicine and Dentistry, Rochester, NY

[3]Division of Allergy, Immunology, Rheumatology, Department of Medicine, University of Rochester School of Medicine and Dentistry, Rochester, NY

Summary

The troponin complex, which consists of three regulatory proteins (troponin C, troponin I and troponin T), is known to regulate muscle contraction in skeletal and cardiac muscle, but its role in smooth muscle remains controversial. Troponin T3 (TnnT3) is a fast skeletal muscle troponin believed to be expressed only in skeletal muscle cells. To determine the in vivo function and tissue specific expression of *Tnnt3*, we obtained the heterozygous *Tnnt3*+/flox/*lacZ* mice from Knockout Mouse Project (KOMP) Repository. *Tnnt3*$^{lacZ/+}$ mice are smaller than their WT littermates throughout development, but do not display any gross phenotypes. *Tnnt3*$^{lacZ/lacZ}$ embryos are smaller than heterozygotes, and die shortly after birth. Histology revealed hemorrhagic tissue in *Tnnt3*$^{lacZ/lacZ}$ liver and kidney, which was not present in *Tnnt3*$^{lacZ/+}$ or WT, but no other gross tissue abnormalities. X-gal staining for *Tnnt3* promoter-driven *lacZ* transgene expression revealed positive staining in skeletal muscle and diapharam, and smooth muscle cells located in the aorta, bladder, and bronchus. Collectively, these findings suggest that troponins are expressed in smooth muscle, and are required for normal growth and breathing for postnatal survival. Moreover, future studies with this mouse model can explore TnnT3 function in adult muscle function using the conditional-inducible gene deletion approach.

Keywords

Troponin; Knockout Mice; Muscle; Development

INTRODUCTION

The troponin (Tnn) complex contains a number of regulatory proteins that control skeletal and cardiac striated muscle contraction. The Tnns are a cooperative complex of three subunits comprised of Troponin T (Tropomyosin interacting subunit, TnnT), Troponin C ([Ca2+] interacting subunit, TnnC), and Troponin I (Inhibitory subunit, TnnI) that function with tropomyosin (Tm) to regulate the interaction of Tm and actin filaments during force

[4]To whom correspondence should be addressed: Dr. Edward M. Schwarz, The Center for Musculoskeletal Research, University of Rochester Medical Center, 601 Elmwood Avenue, Box 665, Rochester, NY 14642, Phone 585-275-3063, FAX 585-756-4727, Edward Schwarz@URMC.Rochester.edu.

NIH-PA Author Manuscript
NIH-PA Author Manuscript
NIH-PA Author Manuscript

NIH-PA Author Manuscript

NIH-PA Author Manuscript

NIH-PA Author Manuscript

generation (el-Saleh, Warber et al. 1986; Szczesna and Potter 2002). Different combinations of Tnn subtypes are expressed in different muscle cells based on their fast or slow muscle phenotype. For example: fast cardiac muscle cells express *Tnnt2*, *Tnni3*, and *Tnnc1*; slow skeletal muscle cells express *Tnnt1, Tnni1*, and *Tnnc1*; and fast skeletal muscle cells express *Tnnt3, Tnni2*, and *Tnnc2*. In contrast, smooth muscle contraction is generally believed to be independent of Tnn regulation based on biochemical studies that failed to indentify these proteins in smooth muscle tissues (Johansson 1987; Jiang and Stephens 1994; Owens 1995; Darland and D'Amore 2001; Watanabe, Yoshino et al. 2003). However, it was recently reported that the fast skeletal *Tnn* genes are required to assemble a functional fast-twitch troponin complex, and their expression and association with tropomyosin-actin filaments in vascular smooth muscle cells has been demonstrated by immunofluorescence microscopy (Moran, Garriock et al. 2008). Thus, the nature of Tnn expression and function in smooth muscle in various tissues is an area of active investigation.

Our interest in Tnn expression and function in smooth muscle was derived from our quest to elucidate the mechanism of flare in rheumatoid arthritis (RA). Using longitudinal contrast enhanced (CE) MRI to study the natural history of knee flare in the tumor necrosis factor-transgenic (TNF-Tg) mouse model of RA (Keffer, Probert et al. 1991), we observed a predictive behavior of the adjacent popliteal lymph nodes (PLN), which increases in size and CE during a prolonged asymptomatic “expanding” phase, prior to a sudden decrease in CE and PLN “collapse” during the onset of arthritic flare (Proulx, Kwok et al. 2007; Proulx, Kwok et al. 2007; Li, Kuzin et al. 2010; Li, Zhou et al. 2011; Li, Ju et al. 2012). As this PLN collapse and knee flare, defined as a significant increase in synovial volume, occurs in the absence of any detectable changes in cellularity or autoimmunity, we performed a microarray gene expression analysis of mRNA isolated from wild-type (WT), TNF-Tg expanding, and TNF-Tg collapsed PLN. The most remarkable finding was the ~100-fold decrease in fast skeletal muscle gene expression, including *Tnnt3*, in expanding PLN versus WT and collapsed PLN. This finding intrigued us, particularly since TnnT3 deficiency in Sheldon-Hall syndrome is characterized by contractures of the distal joints of limbs (Sung, Brassington et al. 2003; Sung, Brassington et al. 2003; Stevenson, Carey et al. 2006; Robinson, Lipscomb et al. 2007; Zhao, Jiang et al. 2011). As subsequent attempts to confirm these differences in mRNA and protein expression in PLN tissue via in situ hybridization and immunohistochemistry failed to produce credible results due to technical issues with probe sensitivity and specificity, we chose to investigate transgene expression of the *Tnnt3*$^{tm2a(KOMP)Wtsi}$ mouse, obtained from the Knock Out Mice Program (KOMP), as a surrogate marker of endogenous *Tnnt3* gene expression. Since this targeted *Tnnt3* gene produces a null mutation, we also analyzed the phenotype of *Tnnt3* heterozygous (*Tnnt3*$^{lacZ/+}$) and homozygous (*Tnnt3*$^{lacZ/lacZ}$) mutant mice.

RESULT AND DISCUSSION

The *Tnnt3*$^{lacZ/+}$ (*Tnnt3*$^{tm2a(KOMP)Wtsi}$) mice in a C57BL/6 background were generated as part of the KOMP using the gene targeting strategy summarized in Figure 1. Central to the purposes of our studies, the targeting vector contains the *lacZ* expressing cassette with polyA tail inserted between Exon 9 and Exon 10, generating a null allele that produces β-galactosidase in cells with active *Tnnt3* gene transcription (Fig. 1A). Although we did not attempt subsequent TnnT3 gain and loss of function studies with this line, the resulting genotypes following crossing with Flp recombinase-expressing (Fig. 1B) and Cre recombinase expressing mice (Fig. 1C) are shown to illustrate the potential of these *Tnnt3*$^{tm2a(KOMP)Wtsi}$ mice.

Standard breeding of *Tnnt3*$^{tm2a(KOMP)Wtsi}$ to C57BL/6 mice produced WT and *Tnnt3*$^{lacZ/+}$ with normal Mendelian distribution. However, an obvious growth delay was observed in

NIH-PA Author Manuscript

NIH-PA Author Manuscript

NIH-PA Author Manuscript

Tnnt3$^{lacZ/+}$ mice assessed as adults at 2 months of age (Fig. 2A), and the mutant mice had a significantly smaller mass as determined by body weight out to 9-weeks (Fig. 2B). In contrast, *Tnnt3*$^{tm2a(KOMP)Wtsi}$ self breeding failed to produce any *Tnnt3*$^{lacZ/lacZ}$ adult mice in >20 litters, although *Tnnt3*$^{lacZ/lacZ}$ pups were found dead a few hours after birth. A gross assessment of embryos harvested on E18.5 revealed that the *Tnnt3*$^{lacZ/lacZ}$ knockouts are smaller than their *Tnnt3*$^{lacZ/+}$ littermates (Fig. 2C & D). These results demonstrate that TnnT3 is required for normal growth and postnatal survival.

To confirm *Tnnt3*gene deletion, *tnnt3*mRNA levels were assessed in WT and *Tnnt3*$^{lacZ/+}$ mice (Fig. 2E), and WT, *Tnnt3*$^{lacZ/+}$ and *Tnnt3*$^{lacZ/lacZ}$ E18.5 embryos (Fig. 2F). As we expected, *tnnt3* were significantly decreased in *Tnnt3*$^{lacZ/+}$ vs. WT mice. Interestingly, mRNA levels of the other fast skeletal troponin components, *tnnc2* and *tnni2*, were also down-regulated in *Tnnt3*$^{lacZ/+}$ mice. Moreover, mRNA levels for *tnnt3, tnnc2* and *tnni2*, were all dramatically decreased in E18.5 embryos, suggesting that these genes are co-regulated at this developmental stage, and that there is no compensation for the loss of *Tnnt3*.

To investigate the expression pattern of *Tnnt3*, X-gal staining was performed on whole mount new born pups (Fig. 3A), and tissue sections (Fig. 3 B–P) of *Tnnt3*$^{lacZ/+}$ and WT littermates. The whole mount staining revealed β-galactosidase activity throughout the animal except the tissues that are not covered by skeletal muscle (Fig. 3A), such as the brown fat (indicated by *), galea aponeurotica (indicated by #) and temporal fascia (indicated by ↑). We also observed very strong β-galactosidase activity in skeletal muscle of the lower limb (Fig. 3G) and the diaphragm (Fig. 3K) from *Tnnt3*$^{lacZ/+}$ mice, which is consistent with high levels of *Tnnt3* expression in these skeletal muscle cells. Moreover, β-galactosidase activity was observed in smooth muscle cells from aorta (Fig. 3H), bladder (Fig. 3I) and bronchus (Fig. 3J) tissues isolated from the *Tnnt3*$^{lacZ/+}$ mice. In contrast, there was no positive staining or β-galactosidase activity in spleen (Fig. 3L), heart (Fig. 3M), brain (Fig. 3N), kidney (Fig.3O), and liver (Fig. 3P) tissues from *Tnnt3*$^{lacZ/+}$mice, or any tissues from the WT littermates (Fig. 3B–F).

To further explore the delayed growth phenotype of *Tnnt3*$^{lacZ/+}$ mice (Fig. 2), we examined the skeletons of WT and *Tnnt3*$^{lacZ/+}$ mice (Fig. 4). X-gal staining revealed that *Tnnt3* is not expressed in bone, bone marrow or joint connective tissue (Fig. 4A), but is highly expressed in the adjacent skeletal muscle (Fig. 4B). Alcian-blue/alizarin-red staining of adult skeletons revealed a subtle phenotype in which the *Tnnt3*$^{lacZ/+}$ mice had more mineralized bone than WT, especially in the ankle, tail, elbow and skull (Fig. 4C). Similarly, *Tnnt3*$^{lacZ/+}$ embryos have more mineralized bone in the skull and spine versus their WT littermates (Fig. 4D). By taking a closer look at the forelimbs (Fig. 4E) and hindlimbs (Fig. 4F), we found that the mutants have normal joint development, with a very modest decrease in limb length. Quantification of the growth plates in E18.5 embryos confirmed this mild phenotype, as the WT was significantly longer vs. TnnT3 $^{lacZ/+}$ (898.87 +/− 14.65 vs.709.39 +/− 67.18 μm (n=4; p=0.008). Similarly, histologic assessment of spinal tissue from WT and Tnnt3 $^{lacZ/+}$ embryos revealed a mild growth phenotype, but no remarkable differences in anatomy, mineralization or matrix composition (Fig. 4G & H). Collectively, these findings are consistent with the mild growth delay in *Tnnt3*$^{lacZ/+}$ mice, which could be caused by improper skeletal loading due to defects in skeletal and some smooth muscles.

To elucidate the postnatal cause of death of *Tnnt3*$^{lacZ/lacZ}$ mice we performed H&E stained histology on heart, lung, liver and kidney from WT (Fig. 5A–D), *Tnnt3*$^{lacZ/+}$ (Fig. 5E–H) and *Tnnt3*$^{lacZ/lacZ}$ (Fig. 5I–L) embryos harvested at E18.5. No abnormalities were detected in any of the heart (Fig. 5I) and lung (Fig. 5J) tissues examined. In contrast, anomalous hemorrhagic tissues were detected in *Tnnt3*$^{lacZ/lacZ}$ liver (Fig. 5K) and kidney (Fig. 5L).

NIH-PA Author Manuscript

NIH-PA Author Manuscript

NIH-PA Author Manuscript

However, based on mouse physiology, it is unlikely that these lesions could cause immediate death after birth (Turgeon and Meloche 2009). Therefore, given the predicted *Tnnt3* expression in diaphragm (Fig. 3K) and bronchus (Fig. 3J) tissue based on the X-gal staining, we conclude that the death of *Tnnt3*$^{lacZ/lacZ}$ mice shortly after birth is due to respiratory distress.

To follow up on our provocative microarray results, we performed X-gal staining of *Tnnt3*$^{lacZ/+}$ PLN and its surrounding tissue. To our chagrin, the results clearly indicate that *Tnnt3* is not expressed in PLN, but is highly expressed in the adjacent skeletal muscle cells that are physically attached by connective tissue (Fig. 6). While this negative find strongly suggests that our microarray results were caused by skeletal muscle tissue contamination of the WT and collapsed PLN, which are harder to dissect than expanding PLN, it also highlights an inconsistency of conventional lymph node anatomy that posits that PLN are embedded in fat (Standring 2005). In contrast, we find that one third of murine PLN are physically attached to skeletal muscle.

In summary, we find that *Tnnt3* is a muscle specific gene in mice, which is required for normal growth and postnatal survival. Although these finding were predicted based on our current knowledge of fast skeletal muscle troponins, we found that the utility of the KOMP derived *Tnnt3*$^{tm2a(KOMP)Wtsi}$ mouse provided us with the most cost-effective approach to bring our preliminary microarray findings to a timely conclusion. Additionally, these mice allowed us to investigate an emerging controversy in the field of muscle biology, and provide indirect evidence of *Tnnt3* expression in smooth muscle cells in aorta, bladder and bronchus. This novel finding warrants follow up studies to formally demonstrate TnnT3 protein expression in smooth muscles cells, and the use of the *Tnnt3*$^{tm2a(KOMP)Wtsi}$ mouse with an appropriate smooth muscle specific Cre expressing line (Grcevic, Pejda et al. 2012) to assess TnnT3 function in this tissue via conditional-inducible gene deletion.

MATERIALS AND METHODS

Animals

Heterozygous *Tnnt3*$^{tm2a(KOMP)Wtsi}$ mice in a C57BL/6 background were generated by the Knock Out Mice Program (KOMP) at the University of California (Project ID# CSD41352), Davis, using the targeting vector described in Figure 1. We obtained these founder mice, and performed the following experiments on their WT, *Tnnt3*$^{lacZ/+}$ and *Tnnt3*$^{lacZ/lacZ}$ progeny under protocols approved by the University of Rochester Committee for Animal Resources.

RNA Analyses

Muscle tissues were collected from the legs of adult (>3-months) WT and *Tnnt3*$^{lacZ/+}$ mice (n=3); and WT, *Tnnt3*$^{lacZ/+}$ and *Tnnt3*$^{lacZ/lacZ}$ E18.5 embryos (n=3); from which total RNA was extracted using the Qiagen RNeasy® Fibrous Tissue Mini Kit (Qiagen, Valencia, CA). The cDNA was prepared by reverse-transcription of the total RNA using the iScript cDNA synthesis kit (BioRad, Hercules, CA). SYBR Green FastMix® (Quanta, Gaithersburg, MD) was used to detect the DNA synthesis in real-time PCR reactions performed in triplicate using the Rotor-Gene Q platform (Qiagen, Valencia, CA). The annealing temperature for the PCR was 59 °C, and the Ct values for the fast skeletal troponins were normalized to β-*actin*. The PCR primer pairs were:

β-*Actin*, F- AGATGTGGATCAGCAAGCAG; R- GCGCAAGTTAGGTTTTGTCA;

tnnt3, F- CCCTCATTGACAGCCACTTT; R- CCTCCTCTCTTCTGGCCTTC;

tnnc2, F- AGGTAGGACCTGGCCTCAG; R- CACCTTTGGGTGGTGGAGT;

NIH-PA Author Manuscript

NIH-PA Author Manuscript

NIH-PA Author Manuscript

tnni2, F- GCTTGAGATCTCAGGATG, R-TCCATGCCAGACTTCTCC;

Tissue Histology

Analysis of E18.5 embryos and whole mount X-gal staining to detect β-galactosidase activity was performed as previously described (Hilton, Tu et al. 2007). Briefly, embryos were harvested and placed in ice-cold PBS, followed by fixation in 0.2% glutaraldehyde overnight at 4°C. The embryos were then incubated overnight at 4°C in the X-gal staining solution (Gold Biotechnology, St Louis, MO), which contains the substrate (0.25 mg/ml), 2mM MgCl2, 0.01% Na Deoxycholate, 0.02% NP-40, 5mM K4Fe(CN)6, and 5mM K3Fe(CN)6.

X-gal staining of frozen tissue sections was performed as previously described (Hilton, Tu et al. 2007). Briefly, the harvested tissues were prefixed in 0.2% glutaraldehyde overnight in 4°C. For adult bone and joint tissues, decalcification was performed in 14% EDTA for 10 days in 4°C. All samples were transferred to a 15% sucrose PBS solution overnight, followed by 30% sucrose PBS solution overnight in 4°C. Afterwards, the samples were mounted in O.C.T mounting medium (Fisher Scientific), snap-frozen in Isopentane/liquid nitrogen, and then stored at −80°C before sectioning. Cryostat sectioning was performed to cut 6 μm thick sections that were post-fixed with 0.2% glutaraldehyde at 4°C for 10min, stained with X-gal solution for 4 hours at room temperature, and counterstained with fast red (Sigma, St. Louis, MO).

For general histology, organ tissues from E18.5 embryos were fixed in 10% neutral buffered formalin, decalcified, paraffin processed and embedded as previously described (Kohn, Dong et al. 2012). Three μm tissue sections were cut, and the sections were stained with hematoxylin and eosin (H&E). Photomicrographs were obtained at 10× magnification with Zeiss Axioskop 40 microscope.

Skeletal prep

The skin and internal organs of adult mice 2-months of age or embryos at E18.5 were removed, and the remaining skeletal and soft tissues were fixed overnight in 95% ethanol, followed by an overnight incubation in acetone, as previously described (Dong, Jesse et al. 2010). Afterwards, the samples were incubated in Alcian Blue/ Alizarin Red staining solution, transferred into 2% KOH, and stored in a 1:1 glycerol/ethanol until they were photographed.

Statistics

Simple pair wise comparisons of WT vs. *Tnnt*$^{3lacZ/+}$ were calculated as mean +/− standard deviation in Microsoft Excel, and the significance was determined using the Student's t-test. For multiple comparisons, ANOVA was performed using GraphPad prism (GraphPad Software, Inc., La Jolla, CA). For all tests, $p<0.05$ was considered significant.

Acknowledgments

The authors would like to thank Ryan Tierney and Sarah Mack for technical assistance with the histology.

This work was supported by research grants from the National Institutes of Health PHS awards (AR048697 to LX; AR054041, AR056702, AI078907, and AR061307 to EMS).

References

Darland DC, D'Amore PA. Cell-cell interactions in vascular development. Curr Top Dev Biol. 2001; 52:107–149. [PubMed: 11529428]

NIH-PA Author Manuscript

NIH-PA Author Manuscript

NIH-PA Author Manuscript

Dong Y, Jesse AM, et al. RBPjkappa-dependent Notch signaling regulates mesenchymal progenitor cell proliferation and differentiation during skeletal development. Development. 2010; 137(9): 1461–1471. [PubMed: 20335360]

el-Saleh SC, Warber KD, et al. The role of tropomyosin-troponin in the regulation of skeletal muscle contraction. J Muscle Res Cell Motil. 1986; 7(5):387–404. [PubMed: 3540004]

Grcevic D, Pejda S, et al. In vivo fate mapping identifies mesenchymal progenitor cells. Stem Cells. 2012; 30(2):187–196. [PubMed: 22083974]

Hilton MJ, Tu X, et al. Tamoxifen-inducible gene deletion reveals a distinct cell type associated with trabecular bone, and direct regulation of PTHrP expression and chondrocyte morphology by Ihh in growth region cartilage. Dev Biol. 2007; 308(1):93–105. [PubMed: 17560974]

Jiang H, Stephens NL. Calcium and smooth muscle contraction. Mol Cell Biochem. 1994; 135(1):1–9. [PubMed: 7816050]

Johansson B. Calcium and regulation of contraction: a short review. J Cardiovasc Pharmacol. 1987; 10(Suppl 1):S9–S13. [PubMed: 2442527]

Keffer J, Probert L, et al. Transgenic mice expressing human tumour necrosis factor: a predictive genetic model of arthritis. EMBO J. 1991; 10(13):4025–4031. [PubMed: 1721867]

Kohn A, Dong Y, et al. Cartilage-specific RBPjkappa-dependent and -independent Notch signals regulate cartilage and bone development. Development. 2012; 139(6):1198–1212. [PubMed: 22354840]

Li J, Ju Y, et al. Efficacy of B cell depletion therapy on joint flare is associated with increased lymphatic flow. Arthritis Rheum. 2012

Li J, Kuzin I, et al. Expanded CD23(+)/CD21(hi) B cells in inflamed lymph nodes are associated with the onset of inflammatory-erosive arthritis in TNF-transgenic mice and are targets of anti-CD20 therapy. J Immunol. 2010; 184(11):6142–6150. [PubMed: 20435928]

Li J, Zhou Q, et al. CD23(+)/CD21(hi) B-cell translocation and ipsilateral lymph node collapse is associated with asymmetric arthritic flare in TNF-Tg mice. Arthritis Res Ther. 2011; 13(4):R138. [PubMed: 21884592]

Moran CM, Garriock RJ, et al. Expression of the fast twitch troponin complex, fTnT, fTnI and fTnC, in vascular smooth muscle. Cell Motil Cytoskeleton. 2008; 65(8):652–661. [PubMed: 18548613]

Owens GK. Regulation of differentiation of vascular smooth muscle cells. Physiol Rev. 1995; 75(3): 487–517. [PubMed: 7624392]

Proulx ST, Kwok E, et al. MRI and quantification of draining lymph node function in inflammatory arthritis. Ann N Y Acad Sci. 2007; 1117:106–123. [PubMed: 17646265]

Proulx ST, Kwok E, et al. Longitudinal assessment of synovial, lymph node, and bone volumes in inflammatory arthritis in mice by in vivo magnetic resonance imaging and microfocal computed tomography. Arthritis Rheum. 2007; 56(12):4024–4037. [PubMed: 18050199]

Robinson P, Lipscomb S, et al. Mutations in fast skeletal troponin I, troponin T, and beta-tropomyosin that cause distal arthrogryposis all increase contractile function. FASEB J. 2007; 21(3):896–905. [PubMed: 17194691]

Standring, S., editor. Gray's Anatomy. 2005.

Stevenson DA, Carey JC, et al. Clinical characteristics and natural history of Freeman-Sheldon syndrome. Pediatrics. 2006; 117(3):754–762. [PubMed: 16510655]

Sung SS, Brassington AM, et al. Mutations in genes encoding fast-twitch contractile proteins cause distal arthrogryposis syndromes. Am J Hum Genet. 2003; 72(3):681–690. [PubMed: 12592607]

Sung SS, Brassington AM, et al. Mutations in TNNT3 cause multiple congenital contractures: a second locus for distal arthrogryposis type 2B. Am J Hum Genet. 2003; 73(1):212–214. [PubMed: 12865991]

Szczesna D, Potter JD. The role of troponin in the Ca(2+)-regulation of skeletal muscle contraction. Results Probl Cell Differ. 2002; 36:171–190. [PubMed: 11892279]

Turgeon B, Meloche S. Interpreting neonatal lethal phenotypes in mouse mutants: insights into gene function and human diseases. Physiol Rev. 2009; 89(1):1–26. [PubMed: 19126753]

NIH-PA Author Manuscript

NIH-PA Author Manuscript

NIH-PA Author Manuscript

Watanabe M, Yoshino Y, et al. Troponin I inhibitory peptide suppresses the force generation in smooth muscle by directly interfering with cross-bridge formation. Biochem Biophys Res Commun. 2003; 307(2):236–240. [PubMed: 12859945]

Zhao N, Jiang M, et al. A novel mutation in TNNT3 associated with Sheldon-Hall syndrome in a Chinese family with vertical talus. Eur J Med Genet. 2011; 54(3):351–353. [PubMed: 21402185]

NIH-PA Author Manuscript

NIH-PA Author Manuscript

NIH-PA Author Manuscript

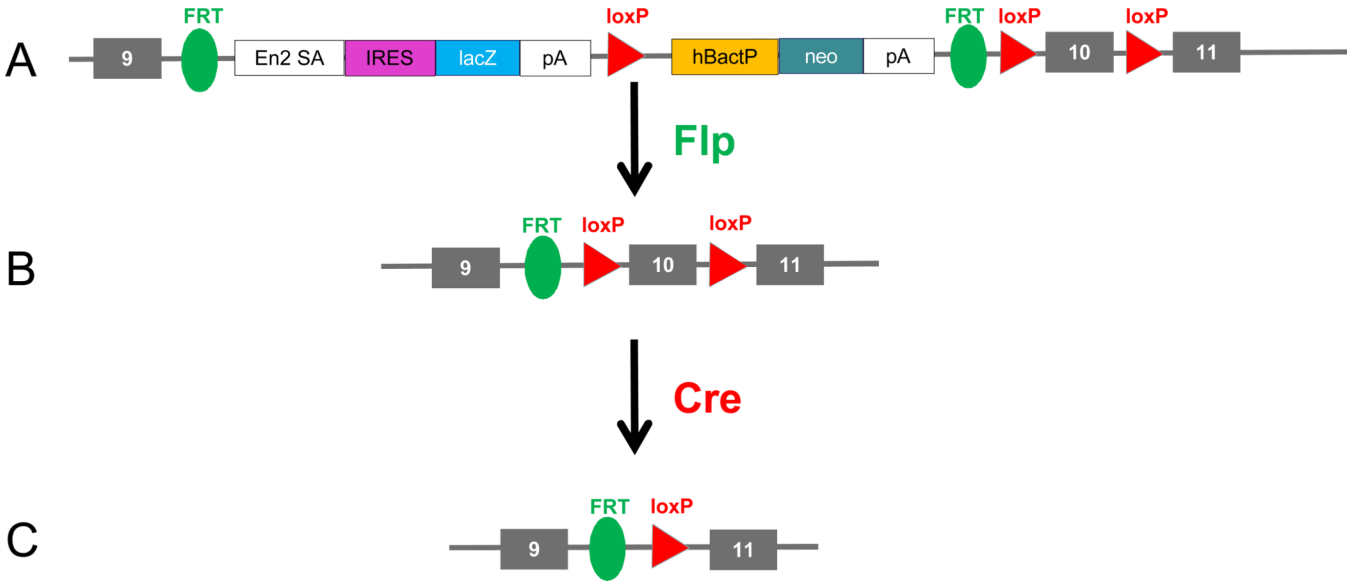

Fig 1. Genomic structure of *Tnnt3*$^{tm2a(KOMP)Wtsi}$ mice

(A) The *Tnnt3/lacZ* knock-in allele (*Tnnt3*$^{tm2a(KOMP)Wtsi}$) is shown to illustrate the mutated *Tnnt3* gene in which the *lacZ* and *neomycin* expression cassette was inserted between Exon 9 and Exon 10, resulting in a *Tnnt3* null gene, and is flanked by FRT (Flippase Recognition Target) sites. This cassette contains the splice acceptor of mouse engrailed 2 exon 2 (En2 SA), an internal ribosome entry sequence (IRES) to initiate *lacZ* translation, and polyadenylation (pA) to terminate transcription after the *lacZ* gene. The *neo* gene is driven by human beta actin promoter (hBactP) and contains it own pA. Additionally, Exon 10 is flanked by loxP sites. (B) The resulting *Tnnt3* conditional knockout gene structure that is generated by crossing *Tnnt3*$^{tm2a(KOMP)Wtsi}$ mice with mice that express the Flp recombinase is shown to illustrate removal of the *lacZ* and neomycin cassette. (C) The resulting *Tnnt3* knockout allele generated after crossing with Cre expression mice is shown.

NIH-PA Author Manuscript
NIH-PA Author Manuscript
NIH-PA Author Manuscript

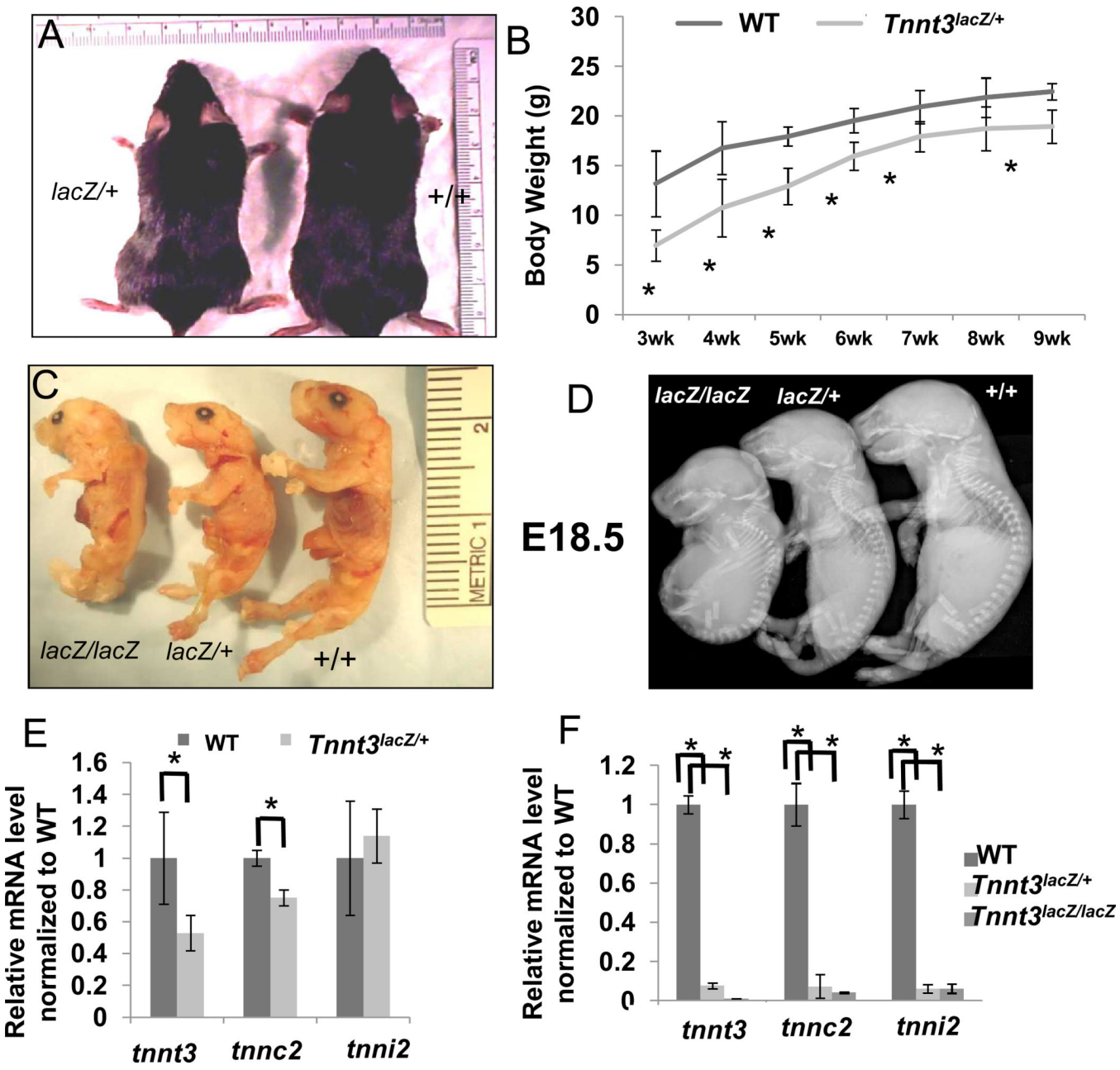

Fig 2. *Tnnt3* is required for postnatal survival, normal growth, and *tnnc2* and *tnni2* expression

(A) The gross phenotype of a representative (n>4) *Tnnt3*$^{lacZ/+}$ mouse at 2 month of age is shown next to its WT (+/+) littermate to illustrate the smaller sized of the mutant animals. Photographs of homozygous (*lacZ/lacZ*) mutant mice could not be obtained since these mice die shortly after birth. (B) The body weights of *Tnnt3* $^{lacZ/+}$ and their WT littermates were measured weekly from 3 to 9 weeks (wk) after birth, and the data are presented as the mean +/− SD (n=4, *p<0.05). A photograph (C) and radiograph (D) of representative *Tnnt3*$^{lacZ/lacZ}$, *Tnnt3*$^{lacZ/+}$ and *Tnnt3*$^{+/+}$ embryos harvested at E18.5 (n≥3) is presented to illustrate the gene dose effect on growth. QRT-PCR was performed on RNA obtained from muscle of WT, *Tnnt3*$^{lacZ/+}$ *or Tnnt3*$^{lacZ/lacZ}$ adult mice (E), or from E18.5 embryos (F), and the data are presented as the mean +/− SD (n=3, *p<0.05).

NIH-PA Author Manuscript
NIH-PA Author Manuscript
NIH-PA Author Manuscript

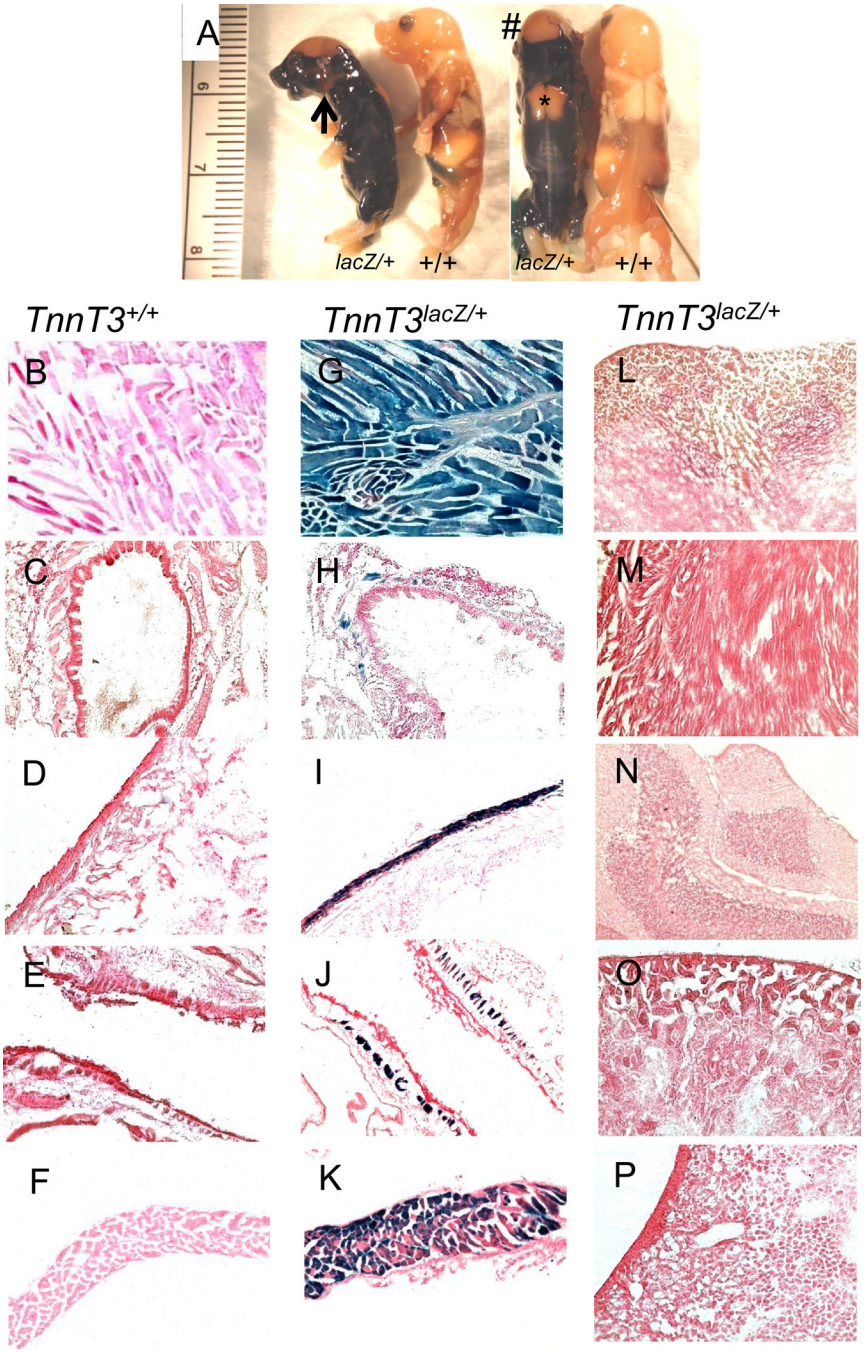

Fig. 3. The tissue specific expression pattern of *Tnnt3*

(A) Whole mount was performed on 1-day old *Tnnt3*$^{lacZ/+}$mice and their WT littermates (n=2). The photograph illustrates the broad X-gal staining in skeletal muscle throughout the *Tnnt3*$^{lacZ/+}$ animal except in brown fat tissue (*), galea aponeurotica (indicated by #) and temporal fascia (indicated by ↑). No β-galactosidase activity was detected in *Tnnt3*$^{+/+}$ mice. (B–P) X-gal staining of tissues from 2 month-old *Tnnt3*$^{lacZ/+}$ mice and WT littermates (n>3), and representative micrographs are show to illustrate the tissue specific expression of the transgene. Note the intense positive staining in skeletal muscle cells next to leg(G) and diaphragm (K), and smooth muscle cells in the aorta (H), bladder (I) and bronchus (J) in the tissues from *Tnnt3*$^{lacZ/+}$ mice. In contrast there was no positive staining in spleen (L), heart

(M), brain (N), kidney (O), and liver (P) tissues from *Tnnt3*$^{lacZ/+}$ mice, or any tissues from the WT littermates.

NIH-PA Author Manuscript
NIH-PA Author Manuscript
NIH-PA Author Manuscript

NIH-PA Author Manuscript
NIH-PA Author Manuscript
NIH-PA Author Manuscript

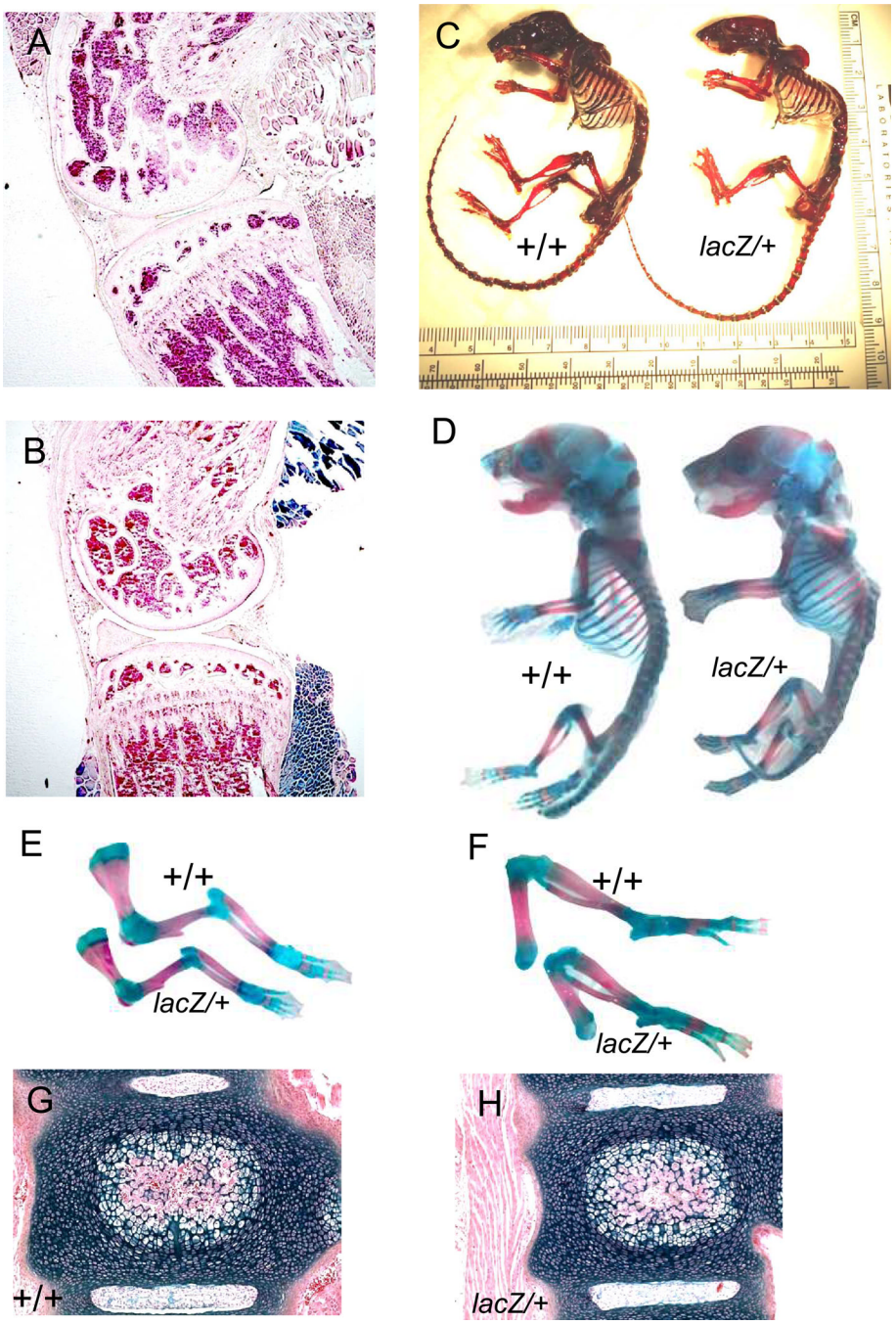

Fig. 4. *Tnnt3* heterozygous mice have a mild skeletal phenotype

X-gal staining was performed on long bones from 2-month-old WT (A) and *Tnnt3*$^{lacZ/+}$ (B) mice (n=3). The micrographs show that the transgene is not expressed in bone, bone marrow or joint connective tissue, but is highly expressed in the adjacent skeletal muscle. (C–F) Alcian-blue/ Alizarin-red staining was performed on the skeletons of 2-month-old (C), and E18.5 embryos (D) of *Tnnt3*$^{lacZ/+}$ and WT mice (n=2) to assess differences in the mineralized (red) and unmineralized (blue) tissue. A closer comparison of the forelimbs (E) and hindlimbs (F) reveals a modest decreased limb length in *Tnnt3*$^{lacZ/+}$ embryos. (G, H) Alcian-blue/Orange G/Alizarin-red staining was performed on histology slides of spinal

tissue from E18.5 embryos of WT (G) and *Tnnt3*$^{lacZ/+}$ (H) mice. No remarkable differences were observed.

NIH-PA Author Manuscript
NIH-PA Author Manuscript
NIH-PA Author Manuscript

NIH-PA Author Manuscript
NIH-PA Author Manuscript
NIH-PA Author Manuscript

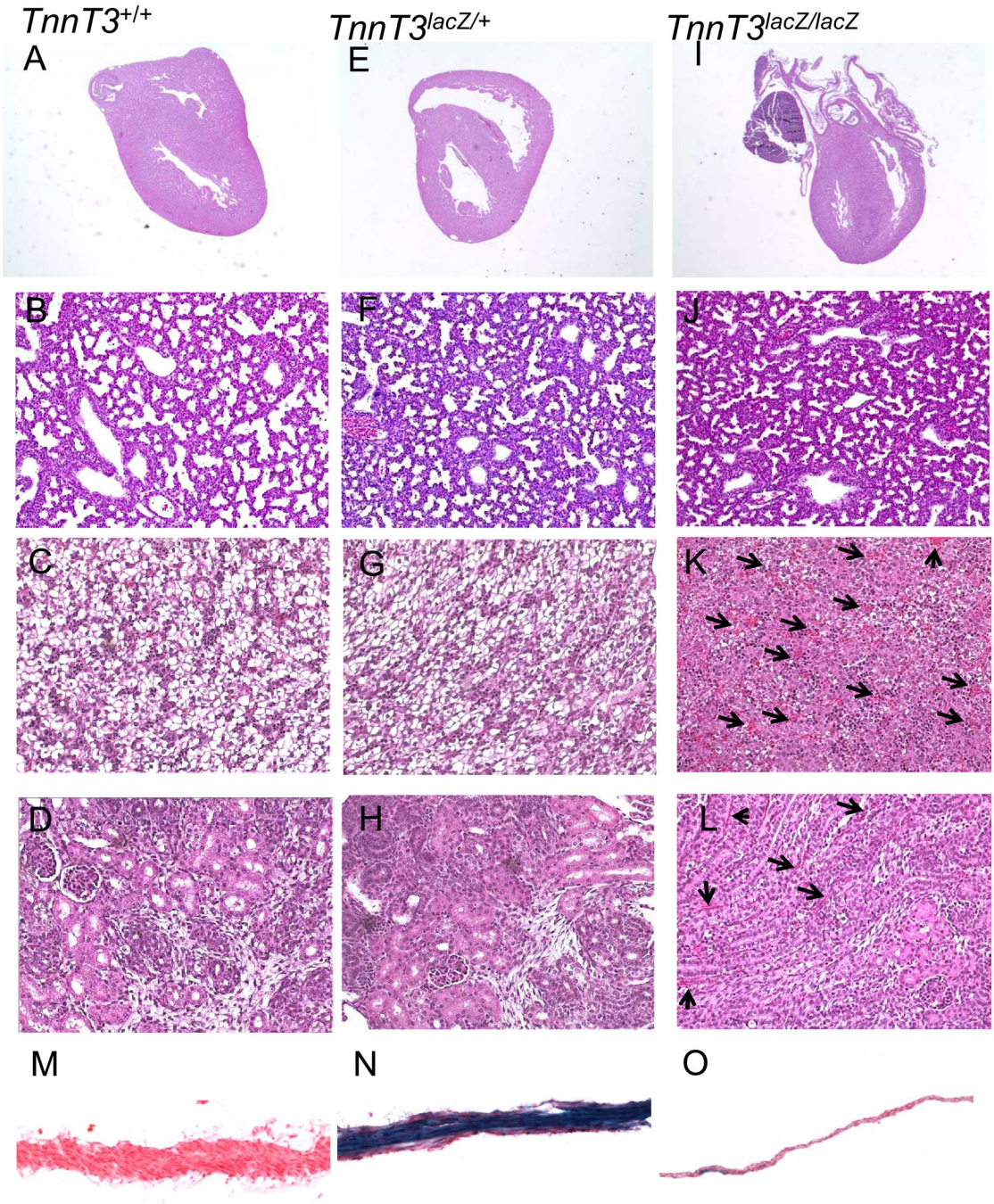

Fig. 5. Histologic evidence of hemorrhage in *Tnnt3*$^{lacZ/lacZ}$ liver and kidney

H&E stained histology was prepared from WT, *Tnnt3*$^{lacZ/+}$ and *Tnnt3*$^{lacZ/lacZ}$ embryos harvested on E18.5. Representative micrographs of heart (A, E, I), Lung (B, F, J), liver (C, G, K) and kidney (D, H, L) tissue are shown. Note the normal appearances of the heart (I) and lung (J) tissue, and the hemorrhagic tissue (arrows) in *Tnnt3*$^{lacZ/lacZ}$ liver (K) and kidney (L). No abnormalities were detected in any of the tissue harvested from WT and *Tnnt3*$^{lacZ/+}$ embryos. Representative histology of diaphragm tissues from WT (M), *Tnnt3*$^{lacZ/+}$ (N) and *Tnnt3*$^{lacZ/lacZ}$ (O) embryos stained with X-gal are also presented to illustrate the markedly thinner diaphragm muscle in the *Tnnt3*$^{lacZ/lacZ}$ embryo.

NIH-PA Author Manuscript
NIH-PA Author Manuscript
NIH-PA Author Manuscript

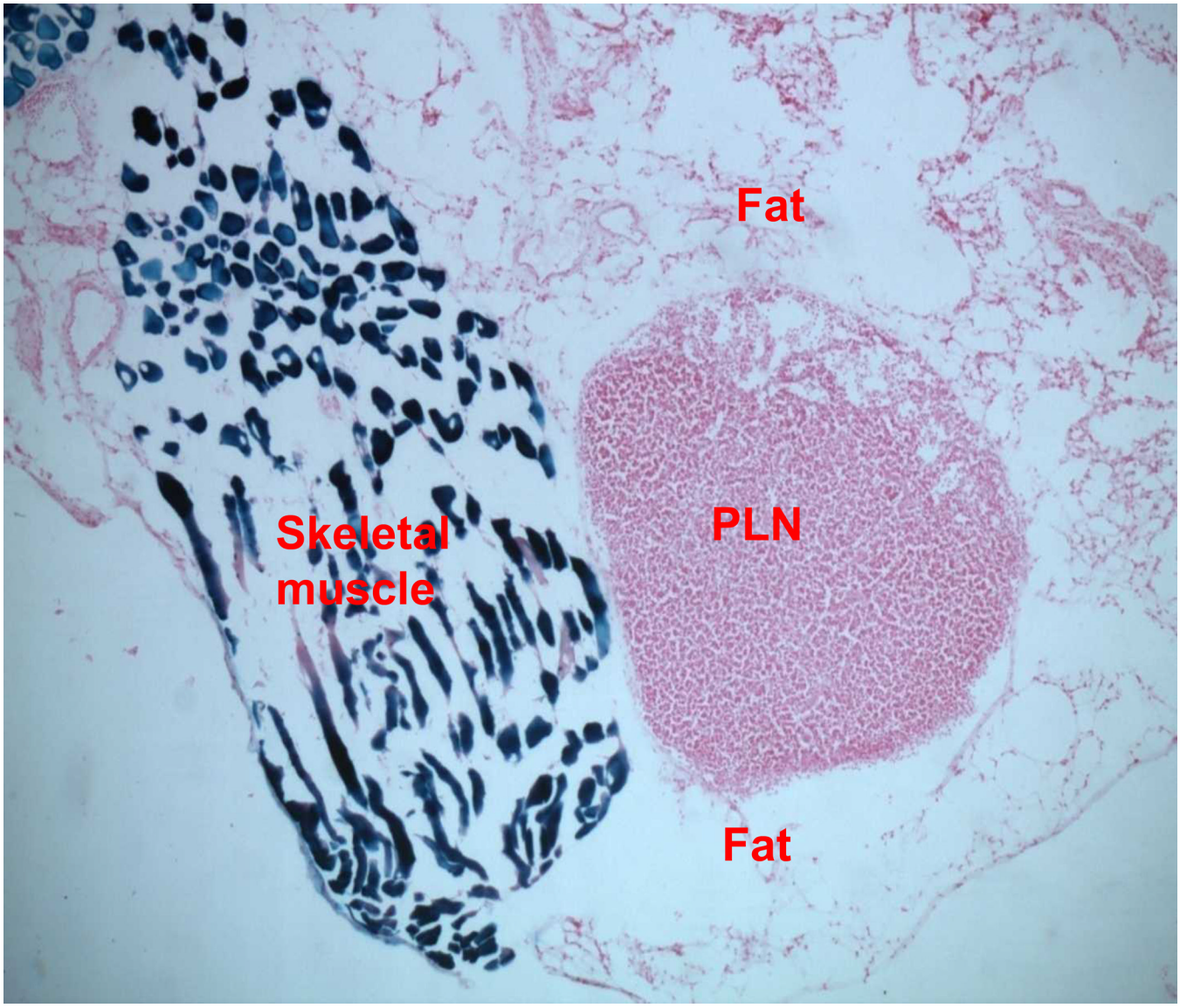

Fig. 6. *Tnnt3* is highly expressed in the skeletal muscle attached to the PLN

X-gal staining of the PLN and surrounding fat and muscle tissue from *Tnnt3*$^{lacZ/+}$ mice reveals that positive staining is only detected in the skeletal muscle.